UvA-DARE (Digital Academic Repository)

Viscoelastic mapping of mouse brain tissue

Relation to structure and age

Antonovaite, N.; Hulshof, L.A.; Hol, E.M.; Wadman, W.J.; Iannuzzi, D.

Link to publication

Research paper

Viscoelastic mapping of mouse brain tissue: Relation to structure and age

Nelda Antonovaite [a],*, Lianne A. Hulshof [b], Elly M. Hol [b,c], Wytse J. Wadman [c], Davide Iannuzzi [a]

[a] *Department of Physics and Astronomy and LaserLaB, VU Amsterdam, The Netherlands*
[b] *Department of Translational Neuroscience, University Medical Center Utrecht, Brain Center, Utrecht University, Utrecht, The Netherlands*
[c] *Center for Neuroscience, Swammerdam Institute for Life Sciences, University of Amsterdam, The Netherlands*

ARTICLE INFO

ABSTRACT

There is growing evidence that mechanical factors affect brain functioning. However, brain components responsible for regulating the physiological mechanical environment are not completely understood. To determine the relationship between structure and stiffness of brain tissue, we performed high-resolution viscoelastic mapping by dynamic indentation of the hippocampus and the cerebellum of juvenile mice brains, and quantified relative area covered by neurons (NeuN-staining), axons (neurofilament NN18-staining), astrocytes (GFAP-staining), myelin (MBP-staining) and nuclei (Hoechst-staining) of juvenile and adult mouse brain slices. Results show that brain subregions have distinct viscoelastic parameters. In gray matter (GM) regions, the storage modulus correlates negatively with the relative area of nuclei and neurons, and positively with astrocytes. The storage modulus also correlates negatively with the relative area of myelin and axons (high cell density regions are excluded). Furthermore, adult brain regions are ∼ 20%–150% stiffer than the comparable juvenile regions which coincide with increase in astrocyte GFAP-staining. Several linear regression models are examined to predict the mechanical properties of the brain tissue based on (immuno)histochemical stainings.

1. Introduction

There is an increasing interest in the mechanical properties of the brain due to the emerging role of physiological mechanical environment in normal brain functioning and involvement of mechanics in disease progression (Barnes et al., 2017). At the single-cell scale, mechanical cues regulate brain development (Franze, 2013), stem cell differentiation (Barnes et al., 2017) and morphology of brain cells (Flanagan et al., 2002; Georges et al., 2006). For instance, axons of neurons grow towards softer tissue *in vivo* (Koser et al., 2016), and adapt their morphology and stiffness to the rigidity of the substrate *in vitro* (Chen et al., 2016). On a tissue scale, there is growing evidence that changes in brain tissue architecture that occur during neuropatho-physiological processes, development, and physiological aging affect the mechanical properties of the brain and thus the local mechanical environment of neurons and glia. To mention a few, reduction of shear modulus was observed during neuroinflammation (Riek et al., 2012), Alzheimer's degeneration (Murphy et al., 2011, 2016), multiple sclerosis (Wuerfel et al., 2010; Fehlner et al., 2015; Streitberger et al., 2011), glial scaring (Moeendarbary et al., 2017) and tumor growth (Jamin et al., 2015; Stewart et al., 2017).

Despite the growing evidence of involvement of mechanical cues in brain functioning, there is a lack of fundamental understanding of how different brain components contribute to the overall stiffness of brain regions. Anatomical regions of the brain differ in their structural composition, from white-matter (WM) regions composed of fiber bundles with varying degree of myelination and thickness to gray-matter (GM) regions with various densities of neurons, glia, and their arborizations. It is thus not surprising that the different brain regions have heterogeneous mechanical properties (Budday et al., 2015; Weickenmeier et al., 2016; van Dommelen et al., 2010; Kaster et al., 2011; Feng et al., 2013; Forte et al., 2017; Christ et al., 2010; Koser et al., 2015; Samadi-Dooki et al., 2017; Finan et al., 2012b; Elkin et al., 2011a; Elkin and Morrison, 2013; Elkin et al., 2010) and that there exists a relationship between some of the components and stiffness (Moeendarbary et al., 2017; Weickenmeier et al., 2016, 2017; Budday et al., 2020). Despite this body of work, how the mechanical properties and structural composition of the brain relate to each other remains elusive.

As multiple brain components are present within each brain region, measurements of mechanical properties while the composition of the brain changes could indicate which brain components regulate the mechanical environment. One of the naturally occurring modifications of brain tissue structure is during postnatal brain development. During this process, the brain undergoes structural changes such as maturation

of extracellular matrix (ECM), myelination, decrease in water content and cell number, dendritic pruning and synaptogenesis, all of which might be accompanied by mechanical alterations (Weickenmeier et al., 2017; Horrocks, 1968; Hammelrath et al., 2016; Sturrock, 1980; Zimmermann and Dours-Zimmermann, 2008; Rauch, 2004). A majority of previous studies have already reported that stiffness increases with maturation (Finan et al., 2012b; Elkin and Morrison, 2013; Elkin et al., 2010; MacManus et al., 2017), yet direct correlations with structural components of measured regions were never investigated. Therefore, the co-quantification of mechanical properties and the composition of the developing brain not only would shed light on structure-stiffness relationship of the brain but also on postnatal maturation of the brain.

In this study, we used a depth-controlled oscillatory indentation technique to map the mechanical properties of individual regions of the hippocampus and cerebellum of horizontal brain slices extracted from juvenile mice (1-month-old). The selected indentation profile enabled viscoelastic characterization in terms of storage and loss moduli, which corresponds to elastic and viscous responses of the material to deformation, respectively, at the tissue scale and physiologically relevant oscillation frequency. Previously, we used the same indentation protocol to map the mechanical properties of adult mouse brain slices, that show that the mechanical properties resemble anatomical regions and that high cell density regions are softer than regions with low cell density, however, the comparison was not quantitative and contributions of other brain components were not addressed (Antonovaite et al., 2018). In the present study, we quantified relative area A_{rel} covered by staining of neurons (NeuN), axons (neurofilament NN18), astrocytes (GFAP), myelin (MBP) and nuclei (Hoechst) of brain sections taken from juvenile (1-month-old) and adult (6–9 months old) mice. Differences as well as correlations between storage modulus and stained components are discussed for adult and juvenile hippocampus.

2. Methods

2.1. Sample preparation for indentation

Two age groups of wild-type (WT) mice (C57BL6/Harlan) were used for indentation experiments: 8 juvenile (1-month-old) and 5 adult (6 and 9-month-old), (for the latter, we refer the reader to Antonovaite et al., 2018). All experiments were performed in accordance with protocols and guidelines approved by the Institutional Animal Care and Use Committee (UvA-DEC) operating under standards set by EU Directive 2010/63/EU. All efforts were made to minimize the suffering and number of animals. The mice were decapitated, the brain was removed from the skull and stored in ice-cold carbogen saturated artificial cerebrospinal fluid (ACSF). Slices were cut in a horizontal plane with a thickness of approximately 300 μm using a VT1200S vibratome (Leica Biosystems, Nussloch, Germany). Slices from 3 to 4 mm of dorsal–ventral positions of the hippocampus were selected for the measurements, where composition along the thickness can be considered homogeneous. After 1 h rest time, single brain tissue slice was placed in a perfusion chamber coated with 0.1% polyethylenimine for adherence between the glass slide and brain slice, stabilized with a harp and supplied with carbogen saturated ACSF solution. Indentation measurements were performed within 8 h at room temperature to avoid mechanical effects of tissue degradation.

2.2. Dynamic indentation setup and measurement protocol

Operation of the custom made indentation setup, including ferrule-top force transducer (Chavan et al., 2012; van Hoorn et al., 2016), has been previously described in detail (Antonovaite et al., 2018, 2020). Indentation mapping was performed in parallel lines with the distance between two adjacent locations of 50 μm, which assured that deformed areas do not overlap. Measurements were carried out on slices from eight mice for the hippocampus and from six mice for cerebellum

with the total number of measurement points $n = 1701$ and $n = 380$, respectively. Previously published oscillatory ramp data on adult mouse brain originated from five mice with the total number of measurement points $n = 1029$ (Antonovaite et al., 2018).

Ferrule-top probes of 0.2–0.5 N/m stiffness and 60–105 μm bead radius were selected for these experiments to have enough resolution to sample individual regions of the brain but also to be able to indent deeper than the surface roughness of the sliced brain tissue which was previously reported to be 1–3 μm (Christ et al., 2010). Indentation-depth controlled oscillatory ramp profile consisted of 0.2 μm amplitude oscillations at 5.62 Hz frequency superimposed on top of a loading ramp at an approximate strain rate of 0.01. The indentation-controlled feedback was triggered at an approximate load of 15 nN, which resulted in the initial uncontrolled 1–3 μm indentation depth, later corrected in post-processing procedures.

2.3. Indentation data analysis

The raw data was analyzed with custom-written MATLAB functions (Antonovaite et al., 2018). Storage E' and loss E'' moduli were calculated according to (Herbert et al., 2008):

$$E'(\omega) = \frac{F_0}{h_0} \cos \delta \frac{\sqrt{\pi}}{2} \frac{(1 - v^2)}{\sqrt{A}}, \tag{1}$$

$$E''(\omega) = \frac{F_0}{h_0} \sin \delta \frac{\sqrt{\pi}}{2} \frac{(1 - v^2)}{\sqrt{A}} \tag{2}$$

where ω is the frequency, F_0 and h_0 are the amplitudes of oscillatory load and indentation-depth, respectively, δ is the phase-shift between indentation and load oscillations, v is the Poisson's ratio (0.5 assuming incompressible material), $A = \pi a^2$ is the contact area. The contact radius a was estimated as $a = \sqrt{hR}$ where h is the indentation depth and R is indenter tip radius.

Indentation depth was converted to the mean strain according to $\varepsilon = 0.2 \times a/R$ (Tabor, 1951), thus mechanical properties were measured in the range between 5 and 8% strain, which fulfills small strain approximation (Lin et al., 2009). While contact adhesion was observed as a pull-off force during retraction, it was not taken into account, as we assume that, under deep indentation conditions, the nominal area dominates over the actual one. Furthermore, it should be noted that contact radius at maximum indentation depth varied between 25 and 42 μm depending on the tip size where the infinite half-space assumption is not fully fulfilled when indenting on narrow regions such as alveus and granular cell layers (GCL). Finally, all indentation curves were checked visually to remove curves where either indentation started in contact or measurements were disturbed by external noise.

2.4. Imaging of 300 μm thickness slices

An inverted microscope (Nikon TMD-Diaphot, Nikon Corporation) was used to image the slice during the indentation measurements with a 2 × magnification objective (Nikon Plan 2X, Nikon Corporation). Images were recorded with a CCD camera (WAT-202B, Watec). After the measurements, the slices were fixed in 4% paraformaldehyde in phosphate buffered saline (PBS) overnight at 4 °C. The slices were stained with Hoechst to label cell nuclei and imaged with Leica DMRE fluorescence microscope (Leica Microsystems, Wetzlar, Germany). Images of the live slices with indentation locations were superimposed on corresponding fluorescent images and each indentation location was assigned to an anatomical region.
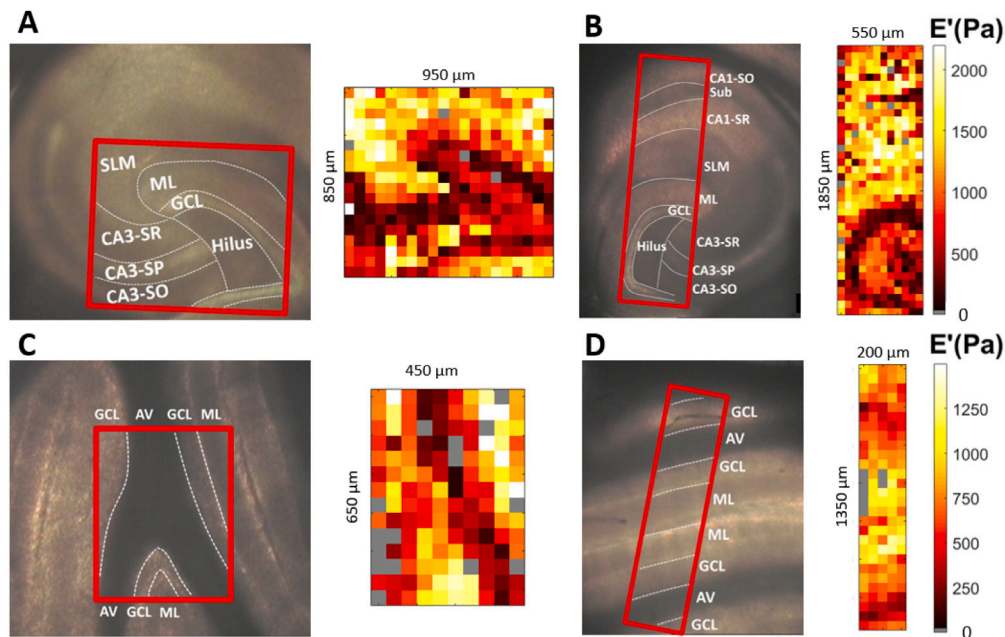
Fig. 1. Microscope images of (A, B) hippocampus and (C, D) cerebellum of 1-month-old mice where area measured by indentation is indicated with red rectangles. Next to it, maps of storage modulus E' at a 50 μm × 50 μm resolution obtained with 0.2 μm oscillation amplitude, 5.62 Hz oscillation frequency, and at 7% strain. The color scale on the top right is for (A, B) and bottom right for (C, D), gray color indicates failed measurements. White lines indicate boundaries of anatomical regions. Abbreviations: Sub — subiculum, SLM — stratum lacunosum moleculare, SR — stratum radiatum, SP — stratum pyramidale, SO — stratum oriens, ML — molecular layer, GCL — granule cell layer, AV — arbor vitae. Gray color indicates failed measurements.

2.5. Imaging and (immuno)histochemistry of 30 μm thickness slices

The separate group of WT mice (C57Bl6/J) were used for (immuno)histochemistry: 3 of each of 1-month-old and 6-month-old. All animals were housed under standard conditions with ad libitum access to water and food. All experiments were approved by the Animal Experimentation Committee of the Utrecht University EU Directive 2010/63/EU.

Mice were anesthetized with 0.1 ml Euthanimal 20% (Alfasan 10020 UDD) and transcardially perfused with 1X PBS. Brains were removed and collected in 4% paraformaldehyde for 48 h before being transferred to 30% sucrose with sodium azide and stored at 4 °C. Before cutting, brains were snapfrozen in isopenthane and embedded in Tissue-Tek (Sakura). Using a cryostat, brains were sliced horizontally in 30 μm thick slices and collected in 1X PBS, which was then replaced by cryopreservation medium (19% glucose, 37.5% ethylene glycol in 0.2 M PB with sodium azide) and stored at −20 °C until further processing.

Slices were washed 3 times with PBS before they were blocked with 10% Normal Donkey Serum (NDS, Jackson ImmunoResearch, 017-000-121) and 0.4% Triton-X in 1X PBS for one hour at RT. Sections were incubated with different primary antibodies (see Table S4) diluted in 200 μl 10% NDS and 0.4% Triton-X blocking medium ON at 4 °C. Thereafter, they were washed 3 times with 1X PBS and then incubated with 1:1000 secondary antibodies or 1:500 Wisteria floribunda agglutinin (WFA) dye diluted in 200 μl 3.3% NDS and 0.13% Triton-X in 1X PBS ON at 4 °C, washed 3 times with 1x PBS and stained with 1:1000 Hoechst dissolved in 500 μl 1x PBS for 10 min at RT. Slices were washed 2 times with 1X PBS and once with MilliQ and mounted with Mowiol (10% Mowiol (Millipore, 475904), 0.1% diazabicyclo(2,2,2)-octane, 0.1 M Tris and 25% glycerol in H_2O; pH 8.5).

Imaging was done with Zeiss Axioscope.A1 epi-microscope operated with AxioVision software, using 10x Plan-NeoFluar objective.

2.6. Image analysis

To compare composition of different anatomical regions, fluorescent images were converted to black and white images by using isodata thresholding algorithm (Fiji software, see Fig. S4 for thresholded images). Relative area fraction A_{rel} of manually identified regions was calculated for each stained component:

$$A_{rel} = \frac{A_{stain}}{A_{region}} \times 100\%, \tag{3}$$

where A_{stain} is area covered with stained component and A_{region} is total area of the region. Images of 8 slices from 3 animals were used for quantification of components. The image analysis was performed using Fiji (ImageJ).

2.7. Linear regression analysis

Linear models were generated by using the *stepwiselm* MATLAB function. The function starts with the constant model and adds parameters as long as it increases statistical power of the model (evaluated based on the change in the sum of squared errors; p-values from F-tests).

2.8. Statistical analysis

Factorial (univariate) ANOVA analysis followed by post hoc tests with bonferroni correction for multiple comparisons was used for statistical analysis of data using IBM SPSS Statistics software.

3. Results

3.1. Mechanical properties of juvenile mouse brain: hippocampus and cerebellum

To characterize local mechanical properties of hippocampus and cerebellum, dynamic indentation mapping was performed on acute mouse brain slices (see Methods 2.1) at 50 μm resolution by indenting with an oscillating ramp at 5.6 Hz frequency up to 8% strain (see Methods 2.2). The viscoelastic properties were quantified in terms of storage E' and loss E'' moduli, and damping factor $\tan(\delta)$, which is the ratio between loss and storage modulus (see Methods 2.3). The brain
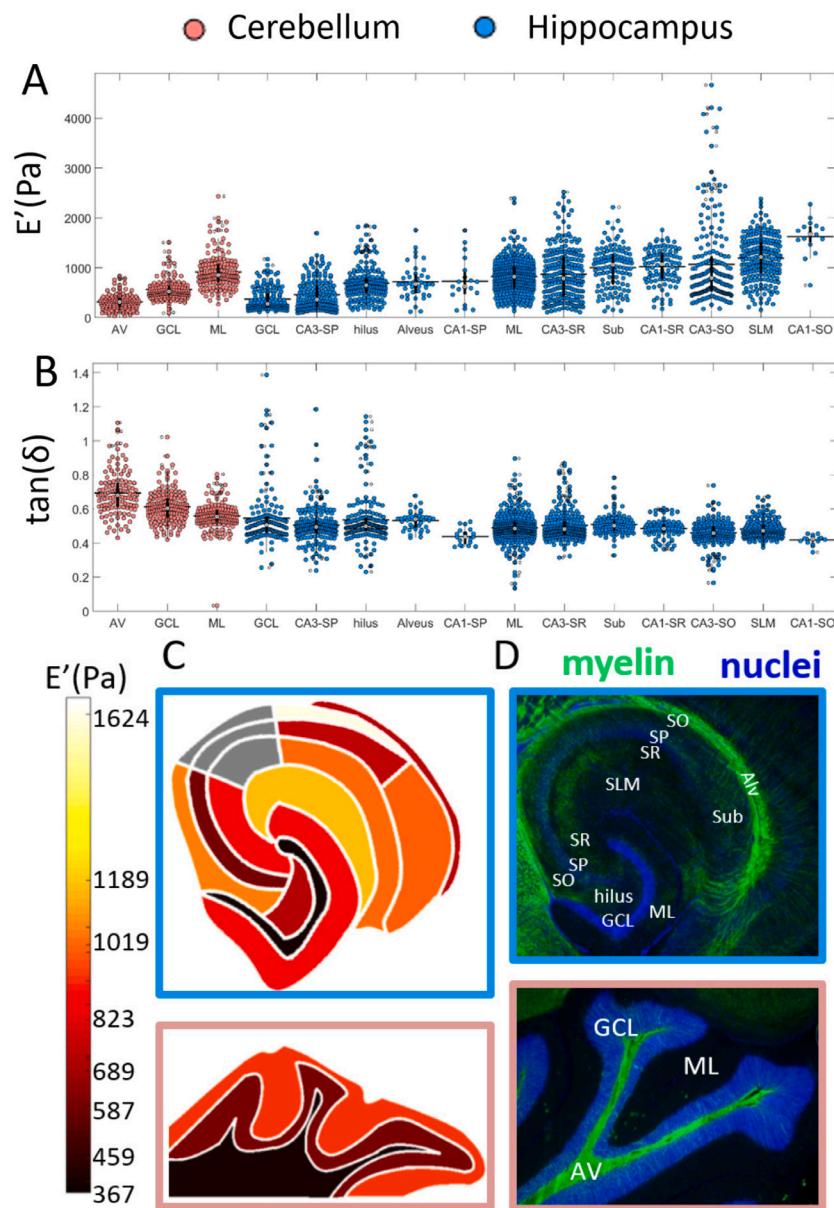
Fig. 2. (A) Storage modulus E' and (B) damping factor $\tan(\delta)$ of regions in cerebellum (red) and hippocampus (blue) of 1-month-old mice ordered from softest to stiffest, obtained at 7% strain and 5.62 Hz frequency of oscillations. The horizontal bar is the mean value, the vertical black bar is 25th and 75th percentiles with median value marked as white dot. Data is pooled from multiple animals (N = 2–6 animals per region and n = 16–335 indentation measurements per region, see Table SS2 for mean values and Fig. S1 for individual animal data). The region, animal and their interaction term were significant factors (factorial ANOVA, p<0.0005 for all factors). (C) Visual reconstruction of mean storage modulus values and (D) fluorescent images of hippocampus and cerebellum stained for nuclei (Hoechst) in blue and myelin (MBP) in green. Scale bar is 500 μm. Abbreviations: Alv — alveus, Sub — subiculum, SLM — stratum lacunosum moleculare, SR — stratum radiatum, SP — stratum pyramidale, SO — stratum oriens, ML — molecular layer, GCL — granule cell layer, AV — arbor vitae.

slices were imaged during dynamic indentation mapping to identify measured anatomical regions (Methods 2.4). Fig. 1 shows two examples of maps of storage modulus of the hippocampus, subregions of DG, CA3 and CA1 (Fig. 1A, B) and two examples of maps of cerebellum (Fig. 1C, D) where lighter color indicates stiffer tissue and darker color indicates softer tissue. Contrast due to mechanical heterogeneity coincided with the shape of anatomically defined brain regions.

To account for the inter-animal variation of mechanical measurements, the same indentation protocol was repeated on slices from multiple animals. The region, animal and their interaction had statistically significant effects for storage modulus and damping factor (factorial ANOVA, p<0.0005 for all factors). For the representation of results, data from different animals was pooled for each anatomical region (Fig. 2A, B). The storage modulus of the hippocampus and cerebellum were mechanically heterogeneous with mean storage modulus

values E' at 7% strain varying from 0.4 to 0.9 kPa in the cerebellum and from 0.4 to 1.6 kPa in the hippocampus (Fig. 2A). The mean damping factor $\tan(\delta)$ was higher in the cerebellum (0.56–0.69) than in the hippocampus (0.42–0.55) (Fig. 2B, p<0.0005 when compared pooled results), indicating higher energy dissipation potential of cerebellum. Fig. 2C shows a color-coded reconstruction of the storage modulus E' of hippocampus and cerebellum, based on the mean results in Fig. 2A, and the fluorescence images of the brain areas stained for nuclei and myelin with identified anatomical regions.

The oscillatory ramp indentation profile allowed us to investigate the strain-dependent mechanical properties of brain tissue i.e. nonlinearity. All brain regions showed an increase in storage modulus E' with strain (see Fig. 3) where stiffening was less pronounced in softer regions (0.04–0.2 kPa vs. 0.2–0.5 kPa per 1% of the strain, respectively). Furthermore, the spread in averaged values was larger at higher strains
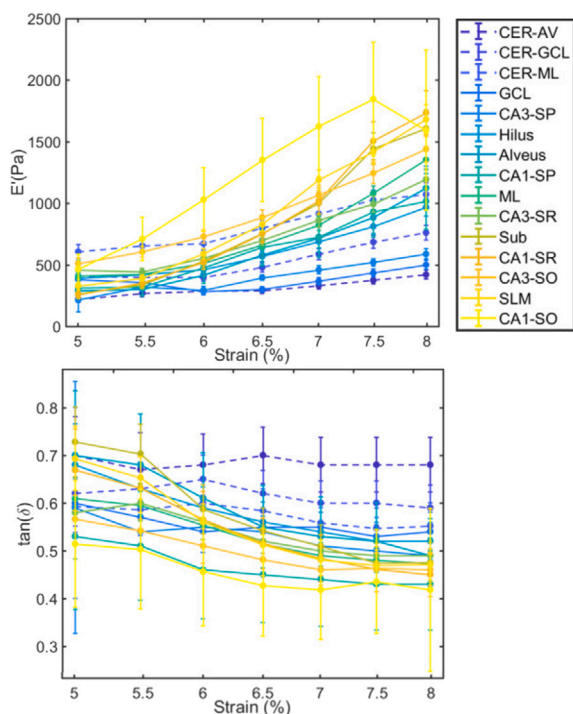
Fig. 3. Mean storage modulus E' and damping factor tan(δ) as a function of strain for different brain regions (see legend) of 1-month-old mice. Dashed lines for cerebellum regions and solid lines for hippocampal regions. Mean ± standard error of the mean (SEM). Note that SEM is positively correlated since the data are not independent.

3.2. Adult brain is stiffer than juvenile brain

The mechanical data from previously obtained hippocampal regions of the adult mouse brain (Antonovaite et al., 2018) was combined with the data from juvenile brain for the comparison (see Fig. 4 for pooled, Fig. S1 and Fig. S2 for individual animal data), where sample preparation, setup, measurement protocols and data analysis were the same. The notable difference was the number of regions: there were 10 regions measured for adult and 15 for juvenile, thus, only regions were used for comparison. The region, age and their interaction terms had statistically significant effects for storage modulus (factorial ANOVA, p<0.0005). The estimated marginal means of the storage modulus E' of adult mouse brain were higher than juvenile mouse brain when comparing all regions together (1.63 ± 0.03 kPa and 0.82 ± 0.02 kPa, respectively) and individually (see Fig. 4 for post hoc test results).

The increase in storage modulus between juvenile and adult mouse brain was lowest and not significant for GCL, CA3-SP and Alveus (20%–50%) which are relatively soft regions and densely packed with either neurons or fibers. Stiffer and less packed regions such as ML and SLM had a higher and significant increase in stiffness with age (60%–150%, see above Fig. 4 p-values from multiple comparisons with Bonferroni correction). The damping factor tan(δ) decreased with age when comparing all regions together (0.51 ± 0.003 and 0.49 ± 0.005, respectively, estimated marginal means ± SE) but at an individual region level it significantly decreased for ML, GCL, hilus and CA3-SR regions, while it increased for CA1-SR (multiple comparisons with Bonferroni correction, p<0.05, 0.0005, 0.0005, 0.05, 0.0005, respectively, see Table SS2 for mean values). These results suggest that during maturation of mouse brain tissue, stiffness of the hippocampus increases while tan(δ) decreases in a region dependent manner.

3.3. Structure-stiffness relationship between brain regions

To assess structural differences between measured brain regions, and between juvenile and adult mouse brains, we performed (immuno)histochemical stainings to label main brain components: all cell nuclei (Hoechst), nuclei of neurons (NeuN), astrocytes (GFAP), axons (neurofilament NN18), myelin (MBP), perineuronal nets (Wisteria floribunda agglutinin WFA) and dendrites (MAP2) (see 5A, staining

(0.2–0.6 kPa at 5% strain and 0.4–1.7 kPa at 8% strain) which means that the contrast in mechanical properties between brain regions is more pronounced at higher strains than at lower strains. The damping factor tan(δ) decreased with strain for regions in the hippocampus (0.03–0.08 per 1% strain), while it was rather constant for cerebellum (decrease of 0.01 per 1% strain), which suggests differential viscoelastic behavior of these two regions.

Fig. 4. Storage modulus E' values of juvenile (red) and adult (blue) hippocampal subregions (data from different slices is pooled, N = 2–6 and n = 16–335 depending on the region, see Table SS2). Gray horizontal bar is mean value, vertical black bar is 25th and 75th percentiles with median value marked as white circle. Statistical differences between juvenile and adult for each region are indicated above (multiple comparisons with Bonferroni correction, ****p<0.0005, ns — non significant). Percentages above the graph are relative increases in mean storage modulus with age.
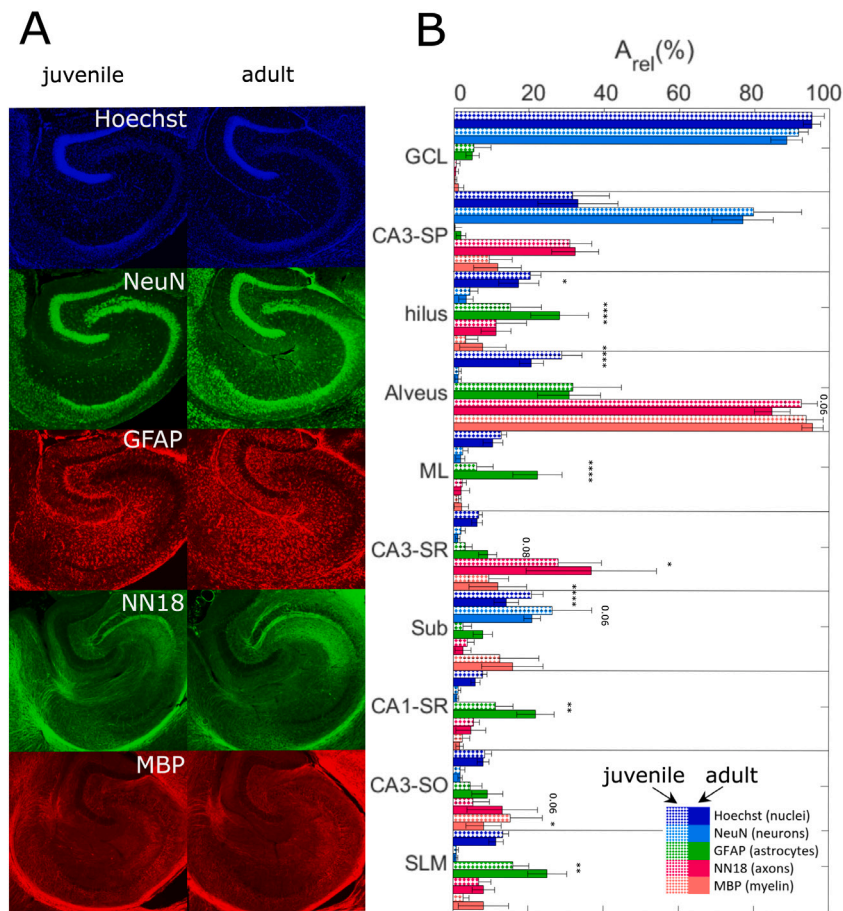
Fig. 5. Comparison of fluorescent images of different brain components between juvenile and adult mice hippocampus. A) Representative fluorescent images of stainings of all cell nuclei (Hoechst), nuclei of neurons (NeuN), astrocytes (GFAP), axons (neurofilament NN18) and myelin (MBP). Dimensions of images are 2065 μm (width) and 1878 μm (height). B)Mean relative area A_{rel}(%), averaged over multiple slices (6–28) obtained from 2–3 animals per age group, of different brain components of juvenile (first bar) and adult (second bar) hippocampal mouse brain regions. Mean ± SD (Table S3). Bonferroni corrected p-values for pairwise comparison of simple main effects are indicated with asterisks (see Table S4): ***p<0.001,**p<0.01, *p<0.05.

procedure in Methods 2.5). The amount of each component was quantified as A_{rel}(%), a relative area covered by the stained component within each region (Fig. 5B, see Table S3 for all A_{rel} values and Methods 2.6 for protocol). MAP2 and WFA stainings were compared qualitatively because they did not show clear regional differences in terms of A_{rel} (Fig. 6).

When comparing juvenile and adult mouse brain stainings, region, age and their interaction term were found to be significant factors for A_{rel} of GFAP and nuclei (factorial ANOVA, p < 0.0005) and not significant for A_{rel} of NeuN, neurofilament NN18 and MBP. A_{rel} of GFAP increased while A_{rel} of nuclei decreased in most of the regions although not all differences were significant (see Fig. 5B, Table S4). Interestingly, increase in storage modulus from juvenile to adult brain ($\Delta E'$) had moderate positive correlation with the increase in A_{rel} of GFAP (Pearson's correlation coefficient r = 0.61, p = 0.06, Fig. 7F) while correlations were weak for all other components (r = −0.18 for Hoechst; 0.4 for NeuN; 0.05 for neurofilament NN18; 0.25 for MBP).

A vast number of WFA positive cells were in the Subiculum while a few cells were WFA positive in the SP layer of CA1-CA3 regions. Comparison between juvenile and adult mouse brains showed a clear increase in perineuronal nets (PNNs) positive cells in Subiculum with age (Fig. 6). Staining with MAP2 of dendrites showed organizational rather than quantitative differences between regions (Fig. 6). Dendrites appeared as a honeycomb structure around cells, parallel and long in CA1-SR and Sub regions and homogeneous in all of the other regions. A comparison between adult and juvenile did not show differences in MAP2 staining.
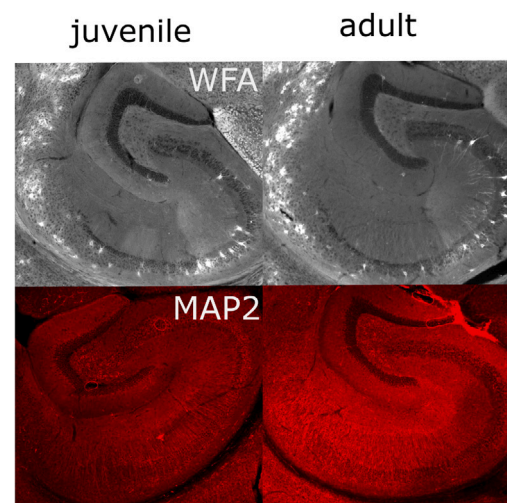
Fig. 6. Representative fluorescent images of (immuno)histochemical stainings of PNNs (WFA) and dendrites (MAP2). Dimensions of images are 2065 μm (width) and 1878 μm (height).

Assessment of mechanical and structural regional differences was done by plotting storage modulus E' as a function of A_{rel} of different brain components, both adult (in blue) and juvenile (in red) (see
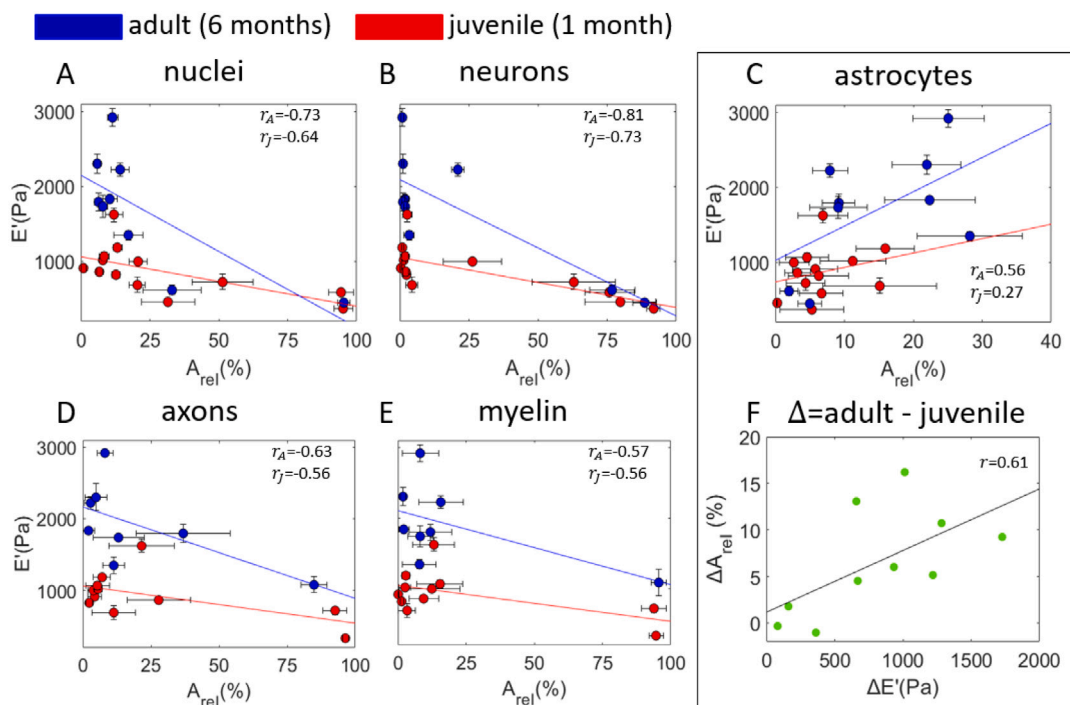
Fig. 7. Storage modulus E' (mean ± SEM) as a function of relative area A_{rel} (mean ± SD) covered by A) all nuclei (Hoechst), B) nuclei of neurons (NeuN), C) astrocytes (GFAP), D) axons (neurofilament NN18) and E) myelin (MBP) of measured regions, both juvenile (red) and adult (blue). WM regions (Alv and AV) are excluded in A–C) plots while high-density GM regions (GCL in hippocampus and cerebellum) are excluded in D–E) plots. Pearson's correlation coefficient identified above, r_a for adult data and r_j for juvenile. F) Increase in A_{rel} of astrocyte staining as a function of the increase in storage modulus E' when comparing juvenile and adult data. Pearson's correlation factor r = 0.61 (p = 0.06).

Fig. 7). As both, high-density cell regions and high-density fiber bundles (WM), are mechanically soft, correlation analysis for nuclei, neurons and astrocytes (Fig. 7A–C) was done by excluding WM regions (Alv and AV) while correlation analysis for myelin and axons (Fig. 7D, E) was done by excluding regions with high-density of nuclei (GCL, SP3 and SP1, A_{rel} > 50%). As a result, E' was found to correlate negatively with A_{rel} of nuclei (Pearson's correlation factor for adult $r_a = -0.73$ and for juvenile $r_j = -0.64$), neurons ($r_a = -0.81$, $r_j = -0.73$), axons ($r_a = -0.57$, $r_j = -0.56$) and myelin ($r_a = -0.63$, $r_j = -0.56$). Moreover, storage modulus E' correlated positively with A_{rel} of astrocytes ($r_a = 0.56$, $r_j = 0.27$). Together, these results show that relatively cell-free and axon-free regions are the stiffest while regions that are tightly packed with either nuclei or axons are the softest, whereas a more pronounced GFAP cytoskeleton in astrocytes seemed to be responsible for higher stiffness values between regions and when comparing juvenile and adult brains.

3.4. Linear regression model for storage modulus prediction from (immuno)histological data

Previous studies have shown that the mechanical properties of spinal cord can be predicted from histological data (Koser et al., 2018, 2015). We applied linear regression analysis (see Methods 2.7) to investigate which of the measured histological parameters are needed for the prediction of storage modulus values of individual brain regions. The best prediction (R^2=0.60) of storage modulus E' of juvenile brain areas, when including indentation data of hippocampus and cerebellum, was achieved with the relative area of NeuN A_{NeuN} (p = 0.002) and GFAP A_{GFAP} (p = 0.01) stainings:

$$E' = a * A_{NeuN} + b * A_{GFAP} + c \qquad (4)$$

where $a = -7.5 \pm 1.9$, $b = -14.9 \pm 5.0$ and $c = 1172 \pm 103$ are linear regression model parameters.

The best prediction ($R^2 = 0.70$) of storage modulus E' of adult brain hippocampal regions was achieved with the relative area of NeuN A_{NeuN} (p = 0.007) and neurofilament NN18 A_{NN18} (p = 0.07) stainings:

$$E' = a * A_{NeuN} + b * A_{NN18} + c \qquad (5)$$

where $a = -17.9 \pm 4.8$, $b = -13.0 \pm 6.2$ and $c = 2230 \pm 220$ are model parameters.

To test whether including other histological parameters would improve the prediction of regional mechanical properties, estimations of densities of cells, neurons, glia, oligodendrocytes, astrocytes and microglia of adult hippocampal regions were acquired from Blue Brain Cell Atlas (BBCA) (for more information Erö et al., 2018). It is important to note that these estimations of cell densities are calculated from the entire volume of the brain region whereas we measured mechanical properties only at the specific plane within the brain. Therefore, by using this data we assumed that there are no variations in cell densities and mechanical properties within the volume of the brain areas. As a result, linear regression model revealed that density of all cells $P_{allcells}$ (p = 5.4×10^{-6}), density of glia P_{glia} (p = 0.01) and relative area of neurofilament NN18 A_{NN18} (p = 0.002) could give the prediction of storage modulus values of hippocampal areas with the highest R-squared value ($R^2 = 0.96$):

$$E' = a * P_{allcells} + b * P_{glia} + c * A_{NN18} + d \qquad (6)$$

where $a = -0.004 \pm 0.0004$, $b = -0.0002 \pm 0.0006$, $c = -13.8 \pm 2.5$ and $d = 2489 \pm 140$ are model parameters.

4. Discussion

4.1. Viscoelastic mapping of hippocampus and cerebellum

In this study, we selected 50 μm mapping resolution and indentation depth of up to 10–17 μm (8% strain) to obtain mechanical properties

of individual regions of hippocampus and cerebellum of the juvenile mouse brain tissue (Fig. 1). We found that both the hippocampus and the cerebellum were mechanically heterogeneous where mechanically distinct regions matched morphologically defined anatomical regions. Similar relative mechanical differences between hippocampal subregions of juvenile mouse brain tissue were found in our previous study on adult mouse brain (Antonovaite et al., 2018) where the measurement protocol was the same as the one in this study. Other studies have been done at different measurement scales and indentation protocols, making it difficult to compare results between studies. For example, some of the studies used tips with the radius of 250 μm resulting in contact area much larger than individual anatomical regions of hippocampus and thus measuring averaged mechanical properties over multiple layers (Budday et al., 2015; Weickenmeier et al., 2016; van Dommelen et al., 2010; Kaster et al., 2011; Finan et al., 2012b; Elkin et al., 2011a; Elkin and Morrison, 2013; Christ et al., 2010; Prange and Margulies, 2002). Other studies used smaller tips and indentation depths (R < 20 μm, h < 4 μm Elkin et al., 2010, 2007; Luque et al., 2016) and reported relative differences between regions different from our findings.

In comparison to studies regarding mechanical properties of the cerebellum, we were able to differentiate between three layers (Fig. 2A), two stiffer GM regions (ML and GCL) and softer WM region (AV), while previous studies only differentiated between GM and WM with contradicting results. Quasi-static indentation measurements with small spherical tips (R = 10-20 μm) agreed with our findings in cerebellum, where GM was stiffer than WM (Christ et al., 2010; Eberle et al., 2018), while stress relaxation measurements, performed with flat cylindrical punch of 250 μm radius, have found that GM was softer than WM (Elkin et al., 2011a) or showed no differences (Finan et al., 2012b; Elkin and Morrison, 2013; Elkin et al., 2011b; Finan et al., 2012a).

It is well-known that the mechanical behavior of the brain tissue is nonlinear and viscoelastic and thus we selected an oscillatory ramp indentation protocol which allowed us to obtain multiple viscoelastic parameters of the brain, i.e. strain-dependent storage modulus E' and damping factor $\tan(\delta)$ (see Fig. 3). These measurements revealed that the cerebellum and the hippocampus have very different viscoelastic properties, i.e. hippocampus showed higher stiffening with strain and had lower damping ratio at higher strains when comparing with the cerebellum. We hypothesize that these differences in mechanical behavior could be related to the fact that cerebellum is folded and located outside of the brain, close to the skull while the hippocampus is positioned in the middle of the brain and does not have folds. These findings demonstrate the potential of measuring multiple mechanical parameters, i.e. storage modulus, damping factor and their depth dependency, as it gives more information about the structure and function of the brain than typical static measurements. For example, a recent study has shown that stiffening with increasing compression is a hallmark for the differentiation between healthy and glioma brain tissue (Pogoda et al., 2014).

Overall, this data can be used to support future biomechanical and biochemical studies. To mention a few, local native mechanical properties of brain tissue are needed when culturing neurons and glial cells on compliant substrates (Flanagan et al., 2002; Georges et al., 2006; Buxboim et al., 2010; Moshayedi et al., 2014; Sur et al., 2013), when designing mechanically compatible brain implants (Spencer et al., 2017) and modeling traumatic brain injuries (Mao et al., 2013; Sáez et al., 2020).

4.2. Changes in mechanical properties of the hippocampus with age

We observed 20%–150% increase in stiffness when comparing juvenile and adult mouse hippocampal regions (Fig. 4), where densely packed regions, either with cells or fibers, stiffened less than loosely packed regions. Furthermore, mechanical damping of hippocampus on average decreased with maturation but changes were much less pronounced than for stiffness (~4%). Our findings confirm most of the previous studies on rodent brain slices. For example, when compared 17–18 postnatal days (PND) and fully mature rat brains, the latter were found to be stiffer for most of the regions (Finan et al., 2012b; Elkin and Morrison, 2013). Another study also found that the elastic modulus of rat hippocampus and cortex increased more than 2 times when comparing prenatal and adult brains (Elkin et al., 2010). In contrast, one study compared the elastic modulus of different brain regions between 10–20 weeks and 100–105 weeks old mice, and only WM in stratum was stiffer (1.5 fold) in older animals (Eberle et al., 2018). Measurements on intact brains rather than brain slices also reported opposing results. For example, 12 weeks old mice were 13%–59% stiffer than 6 weeks old mice (MacManus et al., 2017) while immature rat brains (PND13 and PND17) were stiffer than mature ones (PND43 and PND90) (Gefen et al., 2003). Therefore, our study contributes to the body of evidence that brain tissue stiffens with maturation.

4.3. Changes in (immuno)histochemically stained components of the hippocampus with age

Co-registration of both, mechanical properties and brain components at different developmental stages, could indicate which structural components are responsible for mechanical maturation of brain tissue. Although many structural changes that take place during the maturation of the brain are known, in many cases the data is obtained from large brain regions rather than individual cell layers and limited to the specific development stage, making it difficult to objectively compare the stiffness and composition of brain tissue between different studies. Here, we performed the (immuno)histochemical stainings of brain components (Fig. 4D) of adult and juvenile mouse brain slices, obtained from the same brain areas as slices used for mechanical measurements by using the unique hippocampus shape along the vertical axis to match the slices.

To assess the differences in the cellular composition of hippocampal regions, we stained all cell nuclei (Hoechst), nuclei of neurons (NeuN) and astrocytes (GFAP). Quantification of the relative area covered by stained component of juvenile and adult mouse hippocampus revealed that A_{rel} of GFAP staining significantly increased (1.8–16.2%) with age for most of the subregions, which confirms the previous findings that GFAP is upregulated with maturation of astrocytes and aging of mice (Bushong et al., 2004; Freeman, 2010; Catalani et al., 2002; Clarke et al., 2018). Furthermore, we observed a significant decrease in A_{rel} (0.4%–8%) of nuclei staining (Hoechst) and a non-significant decrease in A_{rel} (0.3%–5%) of neuronal nuclei staining (NeuN) with age for the majority of measured hippocampal subregions. In agreement with our finding, the previous study on mice maturation reported that neuronal and non-neuronal cell nuclei densities decreased in the hippocampus when comparing similar age groups to our study (1 and 4 months) (Fu et al., 2013).

To evaluate the composition of hippocampal regions in terms of cellular arborizations, we stained axons (neurofilament NN18), myelin (MBP) and dendrites (MAP2). When comparing myelin staining (MBP) of juvenile and adult mouse brain slices, A_{rel} was increased (0.8–5.5%) for most of the hippocampal subregions, although the age was not a significant factor. In mice, myelination takes place in the corpus callosum, fimbria and cortex between 1 and 6 months (Horrocks, 1968; Hammelrath et al., 2016; Sturrock, 1980; Suzuki and Raisman, 1994). Although there is no data available of myelination in the mouse hippocampus, it has been reported that, in rats, numbers and distribution of myelinated fibers are the same on day 25 and adulthood (Meier et al., 2004), which agrees with our finding. Furthermore, A_{rel} of axonal staining (neurofilament NN18) was similar between two age groups for most of the hippocampal regions with the exception of Alveus where it was significantly decreased, and CA3-SR and CA3-SO regions, where A_{rel} was significantly increased. Dendritic staining (MAP2) showed no qualitative differences between juvenile and adult hippocampus.

Because neuronal network outgrowth, elongation and branching have been reported to take place in early postnatal stages (P<30), it seems plausible that there are no large structural changes of these networks into the adulthood (Jacobson, 1991; Isaacson, 2012; Pokorný and Yamamoto, 1981; Tamayo et al., 1999; Ziegler and Tavosanis, 2019; Farhy-Tselnicker and Allen, 2018).

Brain tissue also contains ECM which forms a fine macromolecular mesh around cell somata, initial segments of axons, and synapses and consists of collagen type IV, HA, fibronectin, laminin, and proteoglycans (Ruoslahti, 1996; Song and Dityatev, 2018). Because ECM in the brain lacks filamentous proteins such as fibrous collagen type I (Ruoslahti, 1996; Bonneh-Barkay and Wiley, 2009), it is not expected that ECM regulates brain tissue stiffness (Essen, 1997; Haslach et al., 2014). In support of this hypothesis, recently it has been shown that overexpression of ECM components laminin and collagen IV in glial scars correlates with brain tissue softening (Moeendarbary et al., 2017). Nevertheless, during the development of the brain, ECM transitions from a juvenile-type matrix to a mature one (Zimmermann and Dours-Zimmermann, 2008; Rauch, 2004; Milev et al., 1998). To check whether there are differences between 1 and 6 months old hippocampus, we stained perineuronal nets, which are particularly enriched with ECM molecules (Brückner et al., 1993). The noticeable increase in the number of cells wrapped by PNNs was present only in the Subiculum region and thus does not explain the stiffening of all the regions. Previous studies have shown that besides PNNs, hyaluronan/proteoglycan link protein 1 (HAPLN1) increased in the hippocampus between 1.5 and 6 months age (Végh et al., 2014) while protein levels of neurocan, brevican and tenascin-R were similar. Another study has shown that levels of aggrecan, versican (GAGα), brevican increased between 1 and 6 months while levels of neurocan and versican (GAGβ) decreased, although the study was done on the whole volume of rat brains (Milev et al., 1998).

So far, there is very little information regarding the structure-stiffness relationship of the brain tissue during maturation reported in the literature. One previous study has shown that an increase in stiffness of the hippocampus with age (P10, P17 and adult) coincides with the decrease in water content and increase in protein and lipid (myelin) content (Elkin et al., 2010). Another study, although only on white matter, has reported that stiffness tripled while myelin content increased from 58 to 74% when comparing prenatal and postnatal bovine brains (Weickenmeier et al., 2017). The recent study, although using magnetic resonance elastography, has shown an increase in stiffness and decrease in fluidity of the whole hippocampus between 1 and 5 months which was associated with a decrease in number of neuronal precursor cells and immature neurons, increased myelination and change in expression levels of proteins responsible for microtubule formation, myelination, cytoskeleton, cell adhesion, ECM and axonal organization (Guo et al., 2019). In this study, differences in A$_{rel}$ of stained components between juvenile and adult were correlated with differences in storage modulus of individual hippocampal regions rather than the whole hippocampus (Fig. 7F), where only A$_{rel}$ of GFAP staining showed moderate positive correlation, which suggests that GFAP positive cells contribute to mechanical stiffening of hippocampal regions during brain maturation.

One of the limitations of this study is the quantification of the relative area covered by the stained component, which only gives a rough estimate of the brain composition. A more thorough structural analysis could include 3D analysis of brain slices and quantification of size and density of cells, orientation and thickness of cellular arborizations and vasculature, and staining of subtypes of cells, especially for the tightly packed regions. Furthermore, we only investigated structural changes at the tissue scale while changes at cellular/axonal scale might also influence tissue mechanics. Finally, volumetric changes of brain components such as extracellular space or volume fraction of different components could also be important factors governing brain tissue mechanics.

There are two other hypotheses proposed in the literature that explains the cause of brain tissue stiffening with maturation. The first hypothesis implies that, with age, the amount of negatively charged glycosaminoglycans (GAGs) increases (Elkin et al., 2010) resulting in elevated Donan osmotic pressure (Chang and Kaplan, 1977) and thus stiffness, which is similar to the behavior observed in articular cartilage (Sun et al., 2004; Katta et al., 2008). Another hypothesis is that axons in the brain are under tension (Essen, 1997), and axonal tension might increase during brain tissue transition into adulthood. Whether axonal tension or negative charges drive brain tissue stiffening during maturation should be a topic of further investigation.

4.4. Correlation between mechanical properties and (immuno) histochemical stainings

To explain differential mechanical properties of brain regions within the juvenile and adult mouse brains, we performed correlation analysis between relative area covered by (immuno)histochemical staining A$_{rel}$ and storage modulus E'. We found that storage modulus and A$_{rel}$ of all nuclei, nuclei of neurons, axons and myelin of different brain regions have moderate to high negative correlation (Fig. 7A, B, D, E) while A$_{rel}$ of astrocytes has low to moderate positive correlation, with stronger correlation factor for adult than juvenile in all cases. Based on these results, we hypothesize that the loss of myelin as in demyelinating diseases or loss of neurons as during brain development, aging, and neurodegenerative diseases, and increase in the number of astrocytes as in neuroinflammatory diseases would all result in stiffening of the brain region.

One previous study correlated myelin content with the stiffness by comparing different cerebral white matter regions in the bovine brain (myelin content 64%–89%), including pre-natal and post-natal (55%–89%) brain (Weickenmeier et al., 2017). Furthermore, in agreement with our findings, a negative correlation between the density of cell nuclei and shear modulus was shown for human brain tissue although it did not include hippocampus or cerebellum (Budday et al., 2020). Regarding other CNS tissues, it has been shown that cell density and stiffness correlates positively in retinal and spinal cord tissues where contradiction in comparison to our study might be due to differences in CNS tissue composition or much smaller measurement scale (indentation depth <3.5 μm) (Weber et al., 2017; Koser et al., 2015).

4.5. Linear model for predicting mechanical properties of the brain

Prediction of mechanical parameters from histological stainings would allow assessing information about brain stiffness without the need for experimental testing. From the linear regression analysis, we were able to identify that storage modulus could be predicted by using the relative area of NeuN and GFAP staining for the juvenile brain and NeuN and neurofilament NN18 staining for the adult brain. However, the R-squared values of prediction were only 0.6 and 0.7, respectively, questioning the reliability of such a linear model. The prediction of storage modulus of adult mouse hippocampal regions was improved to R-squared of 0.96 by including the density of all cells and glia from Blue Brain Cell Atlas together with the relative area covered by axons. Regarding data from BBCA, the density of all cells was obtained by Nissl staining for all cell bodies. Furthermore, glial staining from BBCA included oligodendrocytes (CNP and MBP), astrocytes (S100b, GFAP and ALDH1L1) and microglia (TMEM119). Therefore, including other parameters describing tissue composition could improve the predictive power of the model. Future studies should investigate which histological parameters are most relevant for describing the structure-stiffness relationship of the brain tissue by expanding it to other brain regions.

5. Conclusions

Dynamic indentation mapping of hippocampus and cerebellum of juvenile mouse brain revealed that viscoelastic parameters vastly differ between individual brain layers. Furthermore, juvenile brain was found to be significantly softer than adult brain. Finally, the constructed structure-stiffness relationships of the brain regions indicated that the observed mechanical differences correlated with the density of several of the identified brain components.

CRediT authorship contribution statement

Nelda Antonovaite: Conceptualization, Methodology, Software, Validation, Formal analysis, Investigation, Resources, Data curation, Visualization, Writing - original draft, Writing - review & editing. **Lianne A. Hulshof:** Investigation, Resources, Writing - review & editing. **Elly M. Hol:** Conceptualization, Writing - review & editing. **Wytse J. Wadman:** Conceptualization, Supervision, Resources, Writing - review & editing. **Davide Iannuzzi:** Conceptualization, Supervision, Funding acquisition, Writing - review & editing.

Declaration of competing interest

One or more of the authors of this paper have disclosed potential or pertinent conflicts of interest, which may include receipt of payment, either direct or indirect, institutional support, or association with an entity in the biomedical field which may be perceived to have potential conflict of interest with this work. For full disclosure statements refer to https://doi.org/10.1016/j.jmbbm.2020.104159. D.I. is co-founder and shareholder of Optics11. N.A. is an employee at Optics11 Life.

Appendix A. Supplementary data

Supplementary material related to this article can be found online at https://doi.org/10.1016/j.jmbbm.2020.104159.

References

Antonovaite, N., Beekmans, S.V., Hol, E.M., Wadman, W.J., Iannuzzi, D., 2018. Regional variations in stiffness in live mouse brain tissue determined by depth-controlled indentation mapping. Sci. Rep. 8.

Antonovaite, N., van Wageningen, T.A., Paardekam, E.J., Dam, A.-M.v., Iannuzzi, D., 2020. Dynamic indentation reveals differential viscoelastic properties of white matter versus gray matter-derived astrocytes upon treatment with lipopolysaccharide. J. Mech. Behav. Biomed. Mater. 109, 103783.

Barnes, J.M., Przybyla, L., Weaver, V.M., 2017. Tissue mechanics regulate brain development, homeostasis and disease. J. Cell Sci. 130 (1), 71–82.

Bonneh-Barkay, D., Wiley, C.A., 2009. Brain extracellular Matrix in Neurodegeneration. Brain Pathol. 19 (4), 573–585.

Brückner, G., Brauer, K., Härtig, W., Wolff, J.R., Rickmann, M.J., Derouiche, A., Delpech, B., Girard, N., Oertel, W.H., Reichenbach, A., 1993. Perineuronal nets provide a polyanionic, glia-associated form of microenvironment around certain neurons in many parts of the rat brain. Glia 8 (3), 183–200.

Budday, S., Nay, R., de Rooij, R., Steinmann, P., Wyrobek, T., Ovaert, T.C., Kuhl, E., 2015. Mechanical properties of gray and white matter brain tissue by indentation. J. Mech. Behav. Biomed. Mater. 46, 318–330.

Budday, S., Sarem, M., Starck, L., Sommer, G., Pfefferle, J., Phunchago, N., Kuhl, E., Paulsen, F., Steinmann, P., Shastri, V.P., Holzapfel, G.A., 2020. Towards microstructure-informed material models for human brain tissue. Acta Biomater. 104, 53–65.

Bushong, E.A., Martone, M.E., Ellisman, M.H., 2004. Maturation of astrocyte morphology and the establishment of astrocyte domains during postnatal hippocampal development. Int. J. Dev. Neurosci. 22 (2), 73–86.

Buxboim, A., Rajagopal, K., Brown, A.E., Discher, D.E., 2010. How deeply cells feel: methods for thin gels. Matter : Inst. Phys. J. 22 (19).

Catalani, A., Sabbatini, M., Consoli, C., Cinque, C., Tomassoni, D., Azmitia, E., Angelucci, L., Amenta, F., 2002. Glial fibrillary acidic protein immunoreactive astrocytes in developing rat hippocampus. Mech. Ageing Dev. 123 (5), 481–490.

Chang, R., Kaplan, L.J., 1977. The Donnan equilibrium and osmotic pressure. J. Chem. Educ. 54 (4), 218.

Chavan, D., van de Watering, T.C., Gruca, G., Rector, J.H., Heeck, K., Slaman, M., Iannuzzi, D., 2012. Ferrule-top nanoindenter: An optomechanical fiber sensor for nanoindentation. Rev. Sci. Instrum. 83 (11), 115110.

Chen, L., Li, W., Maybeck, V., Offenhäusser, A., Krause, H.-J., 2016. Statistical study of biomechanics of living brain cells during growth and maturation on artificial substrates. Biomaterials 106, 240–249.

Christ, A.F., Franze, K., Gautier, H., Moshayedi, P., Fawcett, J., Franklin, R.J.M., Karadottir, R.T., Guck, J., 2010. Mechanical difference between white and gray matter in the rat cerebellum measured by scanning force microscopy. J. Biomech. 43 (15), 2986–2992.

Clarke, L.E., Liddelow, S.A., Chakraborty, C., Münch, A.E., Heiman, M., Barres, B.A., 2018. Normal aging induces A1-like astrocyte reactivity. Proc. Natl. Acad. Sci. USA 115 (8), E1896–E1905.

van Dommelen, J.A.W., van der Sande, T.P.J., Hrapko, M., Peters, G.W.M., 2010. Mechanical properties of brain tissue by indentation: Interregional variation. J. Mech. Behav. Biomed. Mater. 3 (2), 158–166.

Eberle, D., Fodelianaki, G., Kurth, T., Jagielska, A., Möllmert, S., Ulbricht, E., Wagner, K., Taubenberger, A.V., Träber, N., Escolano, J.-C., Franklin, R., Vliet, K.J.V., Guck, J., 2018. Acute but not inherited demyelination in mouse models leads to brain tissue stiffness changes. bioRxiv 449603.

Elkin, B.S., Azeloglu, E.U., Costa, K.D., Morrison, B., 2007. Mechanical heterogeneity of the rat hippocampus measured by atomic force microscope indentation. J. Neurotrauma 24 (5), 812–822.

Elkin, B.S., Ilankova, A., Morrison, B., 2011a. Dynamic, regional mechanical properties of the porcine brain: indentation in the coronal plane. J. Biomech. Eng. 133 (7), 071009.

Elkin, B.S., Ilankovan, A., Morrison, B., 2010. Age-dependent regional mechanical properties of the rat hippocampus and cortex. J. Biomech. Eng. 132 (1), 011010.

Elkin, B.S., Ilankovan, A.I., Morrison, B., 2011b. A detailed viscoelastic characterization of the P17 and Adult Rat Brain. J. Neurotrauma 28 (11), 2235–2244.

Elkin, B.S., Morrison, B., 2013. Viscoelastic properties of the P17 and adult rat brain from indentation in the coronal plane. J. Biomech. Eng. 135 (11), 114507.

Erö, C., Gewaltig, M.-O., Keller, D., Markram, H., 2018. A cell Atlas for the Mouse Brain. Front. Neuroinform. 12.

Essen, D.C.V., 1997. A tension-based theory of morphogenesis and compact wiring in the central nervous system. Nature 385 (6614), 313–318.

Farhy-Tselnicker, I., Allen, N.J., 2018. Astrocytes, neurons, synapses: a tripartite view on cortical circuit development. Neural Dev. 13.

Fehlner, A., Papazoglou, S., McGarry, M., Paulsen, K., Guo, J., Streitberger, K.-J., Hirsch, S., Braun, J., Sack, I., Cerebral multifrequency MR elastography by remote excitation of intracranial shear waves - Fehlner - 2015 - NMR in Biomedicine - Wiley Online Library, URL: https://doi.org/10.1002/nbm.3388, https://onlinelibrary.wiley.com/doi/abs/10.1002/nbm.3388.

Feng, Y., Okamoto, R.J., Namani, R., Genin, G.M., Bayly, P.V., 2013. Measurements of mechanical anisotropy in brain tissue and implications for transversely isotropic material models of white matter. J. Mech. Behav. Biomed. Mater. 23, 117–132.

Finan, J.D., Elkin, B.S., Pearson, E.M., Kalbian, I.L., Morrison, B., 2012a. Viscoelastic properties of the Rat Brain in the sagittal Plane: Effects of anatomical structure and Age. Ann. Biomed. Eng. 40 (1), 70–78.

Finan, J.D., Pearson, E.M., Morrison, B., 2012b. Viscoelastic properties of the rat brain in the horizontal plane. Proc. Int. Res. Counc. Biomech. Inj. Conf. 40, 474–485.

Flanagan, L.A., Ju, Y.-E., Marg, B., Osterfield, M., Janmey, P.A., 2002. Neurite branching on deformable substrates. Neuroreport 13 (18), 2411–2415.

Forte, A.E., Gentleman, S.M., Dini, D., 2017. On the characterization of the heterogeneous mechanical response of human brain tissue. Biomech. Model. Mechanobiol. 16 (3), 907–920.

Franze, K., 2013. The mechanical control of nervous system development. Development (Cambridge, England) 140 (15), 3069–3077.

Freeman, M.R., 2010. Specification and Morphogenesis of Astrocytes. Science 330 (6005), 774–778.

Fu, Y., Rusznák, Z., Herculano-Houzel, S., Watson, C., Paxinos, G., 2013. Cellular composition characterizing postnatal development and maturation of the mouse brain and spinal cord. Brain Struct. Funct. 218 (5), 1337–1354.

Gefen, A., Gefen, N., Zhu, Q., Raghupathi, R., Margulies, S.S., 2003. Age-dependent changes in material properties of the brain and braincase of the rat. J. Neurotrauma 20 (11), 1163–1177.

Georges, P.C., Miller, W.J., Meaney, D.F., Sawyer, E.S., Janmey, P.A., 2006. Matrices with compliance comparable to that of brain tissue select neuronal over glial growth in mixed cortical cultures. Biophys. J. 90 (8), 3012–3018.

Guo, J., Bertalan, G., Meierhofer, D., Klein, C., Schreyer, S., Steiner, B., Wang, S., Vieira da Silva, R., Infante-Duarte, C., Koch, S., Boehm-Sturm, P., Braun, J., Sack, I., 2019. Brain maturation is associated with increasing tissue stiffness and decreasing tissue fluidity. Acta Biomater. 99, 433–442.

Hammelrath, L., Škokić, S., Khmelinskii, A., Hess, A., van der Knaap, N., Staring, M., Lelieveldt, B.P.F., Wiedermann, D., Hoehn, M., 2016. Morphological maturation of the mouse brain: An in vivo MRI and histology investigation. NeuroImage 125 (Supplement C), 144–152.

Haslach, H.W., Leahy, L.N., Riley, P., Gullapalli, R., Xu, S., Hsieh, A.H., 2014. Solid–extracellular fluid interaction and damage in the mechanical response of rat brain tissue under confined compression. J. Mech. Behav. Biomed. Mater. 29, 138–150.

Herbert, E.G., Oliver, W.C., Pharr, G.M., 2008. Nanoindentation and the dynamic characterization of viscoelastic solids. J. Phys. D: Appl. Phys. 41 (7), 074021.

van Hoorn, H., Kurniawan, N.A., Koenderink, G.H., Iannuzzi, D., 2016. Local dynamic mechanical analysis for heterogeneous soft matter using ferrule-top indentation Electronic supplementary information (ESI) available. Soft Matter 12 (12), 3066–3073, See DOI: http://dx.doi.org/10.1039/c6sm00300a Click here for additional data file.

Horrocks, L.A., 1968. Composition of Mouse Brain Myelin during Development. J. Neurochem. 15 (6), 483–488.

Isaacson, R., 2012. The Hippocampus: Volume 1: Structure and Development. Springer Science & Business Media, Google-Books-ID: U1jaBwAAQBAJ.

Jacobson, M., 1991. Developmental Neurobiology. Plenum Press.

Jamin, Y., Boult, J.K.R., Li, J., Popov, S., Garteiser, P., Ulloa, J.L., Cummings, C., Box, G., Eccles, S.A., Jones, C., Waterton, J.C., Bamber, J.C., Sinkus, R., Robinson, S.P., 2015. Exploring the biomechanical properties of brain malignancies and their pathologic determinants In Vivo with Magnetic resonance Elastography. Cancer Res. 75 (7), 1216–1224.

Kaster, T., Sack, I., Samani, A., 2011. Measurement of the hyperelastic properties of ex vivo brain tissue slices. J. Biomech. 44 (6), 1158–1163.

Katta, J., Stapleton, T., Ingham, E., Jin, Z.M., Fisher, J., 2008. The effect of glycosaminoglycan depletion on the friction and deformation of articular cartilage. Proc. Inst. Mech. Eng. H 222 (1), 1–11.

Koser, D.E., Moeendarbary, E., Hanne, J., Kuerten, S., Franze, K., 2015. CNS cell distribution and Axon orientation determine local spinal cord mechanical properties. Biophys. J. 108 (9), 2137–2147.

Koser, D.E., Moeendarbary, E., Kuerten, S., Franze, K., 2018. Predicting local tissue mechanics using immunohistochemistry. bioRxiv 358119.

Koser, D.E., Thompson, A.J., Foster, S.K., Dwivedy, A., Pillai, E.K., Sheridan, G.K., Svoboda, H., Viana, M., da F. Costa, L., Guck, J., Holt, C.E., Franze, K., 2016. Mechanosensing is critical for axon growth in the developing brain. Nat. Neurosci. 19 (12), 1592–1598.

Lin, D.C., Shreiber, D.I., Dimitriadis, E.K., Horkay, F., 2009. Spherical indentation of soft matter beyond the Hertzian regime: numerical and experimental validation of hyperelastic models. Biomech. Model. Mechanobiol. 8 (5), 345–358.

Luque, T., Kang, M.S., Schaffer, D.V., Kumar, S., 2016. Microelastic mapping of the rat dentate gyrus. R. Soc. Open Sci. 3 (4).

MacManus, D.B., Pierrat, B., Murphy, J.G., Gilchrist, M.D., 2017. Region and species dependent mechanical properties of adolescent and young adult brain tissue. Sci. Rep. 7.

Mao, H., Elkin, B.S., Genthikatti, V.V., Morrison, B., Yang, K.H., 2013. Why is CA3 more vulnerable than CA1 in experimental models of controlled cortical impact-induced Brain Injury?. J. Neurotrauma 30 (17), 1521–1530.

Meier, S., Bräuer, A., Heimrich, B., Nitsch, R., Savaskan, N., 2004. Myelination in the Hippocampus during Development and Following Lesion, Vol. 61. http://dx.doi.org/10.1007/s00018-004-3469-5.

Milev, P., Maurel, P., Chiba, A., Mevissen, M., Popp, S., Yamaguchi, Y., Margolis, R.K., Margolis, R.U., 1998. Differential regulation of expression of hyaluronan-binding proteoglycans in developing brain: aggrecan, versican, neurocan, and brevican. Biochem. Biophys. Res. Commun. 247 (2), 207–212.

Moeendarbary, E., Weber, I.P., Sheridan, G.K., Koser, D.E., Soleman, S., Haenzi, B., Bradbury, E.J., Fawcett, J., Franze, K., 2017. The soft mechanical signature of glial scars in the central nervous system. Nature Commun. 8, ncomms14787.

Moshayedi, P., Ng, G., Kwok, J.C.F., Yeo, G.S.H., Bryant, C.E., Fawcett, J.W., Franze, K., Guck, J., 2014. The relationship between glial cell mechanosensitivity and foreign body reactions in the central nervous system. Biomaterials 35 (13), 3919–3925.

Murphy, M.C., Huston, J., Jack, C.R., Glaser, K.J., Manduca, A., Felmlee, J.P., Ehman, R.L., 2011. Decreased brain stiffness in Alzheimer's disease determined by magnetic resonance elastography. J. Magn. Reson. Imaging 34 (3), 494–498.

Murphy, M.C., Jones, D.T., Jack, C.R., Glaser, K.J., Senjem, M.L., Manduca, A., Felmlee, J.P., Carter, R.E., Ehman, R.L., Huston, J., 2016. Regional brain stiffness changes across the Alzheimer's disease spectrum. NeuroImage: Clin. 10, 283–290.

Pogoda, K., Chin, L., Georges, P.C., Byfield, F.J., Bucki, R., Kim, R., Weaver, M., Wells, R.G., Marcinkiewicz, C., Janmey, P.A., 2014. Compression stiffening of brain and its effect on mechanosensing by glioma cells. New J. Phys. 16, 075002.

Pokorný, J., Yamamoto, T., 1981. Postnatal ontogenesis of hippocampal CA1 area in rats. i. Development of dendritic arborisation in pyramidal neurons. Brain Res. Bull. 7 (2), 113–120.

Prange, M.T., Margulies, S.S., 2002. Regional, directional, and Age-Dependent properties of the Brain Undergoing Large Deformation. J. Biomech. Eng. 124 (2), 244–252.

Rauch, U., 2004. Extracellular matrix components associated with remodeling processes in brain. Cell. Mol. Life Sci.: CMLS 61 (16), 2031–2045.

Riek, K., Millward, J.M., Hamann, I., Mueller, S., Pfueller, C.F., Paul, F., Braun, J., Infante-Duarte, C., Sack, I., 2012. Magnetic resonance elastography reveals altered brain viscoelasticity in experimental autoimmune encephalomyelitis. NeuroImage: Clin. 1 (1), 81–90.

Ruoslahti, E., 1996. Brain extracellular matrix. Glycobiology 6 (5), 489–492.

Sáez, P., Duñó, C., Sun, L.Y., Antonovaite, N., Malvè, M., Tost, D., Goriely, A., 2020. Topological features dictate the mechanics of the mammalian brains. Int. J. Mech. Sci. 187, 105914.

Samadi-Dooki, A., Voyiadjis, G.Z., Stout, R.W., 2017. An indirect indentation method for evaluating the Linear viscoelastic properties of the brain tissue. J. Biomech. Eng. 139 (6).

Song, I., Dityatev, A., 2018. Crosstalk between glia, extracellular matrix and neurons. Brain Res. Bull. 136, 101–108.

Spencer, K.C., Sy, J.C., Ramadi, K.B., Graybiel, A.M., Langer, R., Cima, M.J., 2017. Characterization of mechanically matched hydrogel coatings to improve the biocompatibility of Neural Implants. Sci. Rep. 7 (1), 1952.

Stewart, D.C., Rubiano, A., Dyson, K., Simmons, C.S., 2017. Mechanical characterization of human brain tumors from patients and comparison to potential surgical phantoms. PLOS ONE 12 (6), e0177561.

Streitberger, K.-J., Wiener, E., Hoffmann, J., Freimann, F.B., Klatt, D., Braun, J., Lin, K., McLaughlin, J., Sprung, C., Klingebiel, R., Sack, I., In vivo viscoelastic properties of the brain in normal pressure hydrocephalus - Streitberger - 2011 - NMR in Biomedicine - Wiley Online Library, URL: https://doi.org/10.1002/nbm.1602, https://onlinelibrary.wiley.com/doi/10.1002/nbm.1602.

Sturrock, R.R., 1980. Myelination of the Mouse Corpus Callosum. Neuropathol. Appl. Neurobiol. 6 (6), 415–420.

Sun, D.D., Guo, X.E., Likhitpanichkul, M., Lai, W.M., Mow, V.C., 2004. The influence of the fixed negative charges on mechanical and electrical behaviors of articular cartilage under unconfined compression. J. Biomech. Eng. 126 (1), 6–16.

Sur, S., Newcomb, C.J., Webber, M.J., Stupp, S.I., 2013. Tuning supramolecular mechanics to guide neuron development. Biomaterials 34 (20), 4749–4757.

Suzuki, M., Raisman, G., 1994. Multifocal pattern of postnatal development of the macroglial framework of the rat fimbria. Glia 12 (4), 294–308.

Tabor, D., 1951. The Hardness of Metals. Clarendon Press, Oxford, URL: https://trove.nla.gov.au/work/12462313.

Tamayo, P., Slonim, D., Mesirov, J., Zhu, Q., Kitareewan, S., Dmitrovsky, E., Lander, E.S., Golub, T.R., 1999. Interpreting patterns of gene expression with self-organizing maps: Methods and application to hematopoietic differentiation. Proc. Natl. Acad. Sci. USA 96 (6), 2907–2912.

Végh, M.J., Heldring, C.M., Kamphuis, W., Hijazi, S., Timmerman, A.J., Li, K.W., van Nierop, P., Mansvelder, H.D., Hol, E.M., Smit, A.B., van Kesteren, R.E., 2014. Reducing hippocampal extracellular matrix reverses early memory deficits in a mouse model of Alzheimer's disease. Acta Neuropathol. Commun. 2, 76.

Weber, I., Yun, S.-H., Scarcelli, G., Franze, K., 2017. The role of cell body density in ruminant retina mechanics assessed by atomic force and Brillouin microscopy. Phys. Biol..

Weickenmeier, J., de Rooij, R., Budday, S., Ovaert, T.C., Kuhl, E., 2017. The mechanical importance of myelination in the central nervous system. J. Mech. Behav. Biomed. Mater. 76 (Supplement C), 119–124.

Weickenmeier, J., de Rooij, R., Budday, S., Steinmann, P., Ovaert, T.C., Kuhl, E., 2016. Brain stiffness increases with myelin content. Acta Biomater. 42, 265–272.

Wuerfel, J., Paul, F., Beierbach, B., Hamhaber, U., Klatt, D., Papazoglou, S., Zipp, F., Martus, P., Braun, J., Sack, I., 2010. MR-elastography reveals degradation of tissue integrity in multiple sclerosis. Neuroimage 49 (3), 2520–2525.

Ziegler, A.B., Tavosanis, G., 2019. Glycerophospholipids – Emerging players in neuronal dendrite branching and outgrowth. Dev. Biol. 451 (1), 25–34.

Zimmermann, D.R., Dours-Zimmermann, M.T., 2008. Extracellular matrix of the central nervous system: from neglect to challenge. Histochem. Cell Biol. 130 (4), 635–653.